APPLIED SCIENCES AND ENGINEERING

Three-dimensional microarchitected materials and devices using nanoparticle assembly by pointwise spatial printing

Mohammad Sadeq Saleh, Chunshan Hu, Rahul Panat*

Three-dimensional (3D) hierarchical materials are important to a wide range of emerging technological applications. We report a method to synthesize complex 3D microengineered materials, such as microlattices, with nearly fully dense truss elements with a minimum diameter of approximately 20 μm and having high aspect ratios (up to 20:1) without using any templating or supporting materials. By varying the postprocessing conditions, we have also introduced an additional control over the internal porosity of the truss elements to demonstrate a hierarchical porous structure with an overall void size and feature size control of over five orders of magnitudes in length scale. The method uses direct printing of nanoparticle dispersions using the Aerosol Jet technology in 3D space without templating or supporting materials followed by binder removal and sintering. In addition to 3D microlattices, we have also demonstrated directly printed stretchable interconnects, spirals, and pillars. This assembly method could be implemented by a variety of microdroplet generation methods for fast and large-scale fabrication of the hierarchical materials for applications in tissue engineering, ultralight or multifunctional materials, microfluidics, and micro-optoelectronics.

INTRODUCTION

Materials with three-dimensional (3D) architectures, such as micro/nanolattices and scaffolds, are of high current interest (*1*) because they can exhibit extraordinary material properties and functionalities in diverse applications, such as biomedical implants (*2*), porous membranes (*3*), load-bearing structures (*4*), microfluidic devices (*5*), fast-charging and high-capacity batteries (*6*), and supercapacitors (*7*). Such microengineered materials have been realized by a variety of techniques and methods, such as two-photon lithography (*4*), projection microstereolithography of polymers (*8*, *9*), and the use of a polymer opal templating (*10*), followed by deposition of suitable materials, such as metals or ceramics over the polymer template (*4*, *8*, *10*). The available techniques to deposit over the template (for example, atomic layer deposition, electroless deposition, or electrodeposition) allow a variety of ceramics and metals to be used in these methods. The polymer is then removed by burnout or by chemical dissolution after the structure is built up. The final product consists of hollow tubes and their composites for truss elements that form the complex 3D scaffold. Although the template fabrication and the material deposition steps are additive, the removal of the underlying template adds a fabrication step, requires the use of chemicals, and creates waste.

Free-form fabrication by printing of nanoparticle solutions and inks followed by sintering is a relatively recent area that has gained importance in the fabrication of a diverse set of electronic devices and materials (*11*, *12*). Printing of nanoparticles over the surfaces of 3D components, such as hemispherical domes (*11*) or pillars (*13*), has been demonstrated for antenna applications. A continuous dispense of nanoparticle dispersion from a micronozzle was used to make nonintersecting structures/motifs in 3D (*12*). Other nozzle-based methods (*14*) use nanoparticles dispersed in viscoelastic inks, which leads to a significant matrix filler between the particles, limiting the part density. Three-dimensional conductive polymer-metal hybrid structures were fabricated by adding silver nitrate to a photocurable oligomer in the presence of suitable photoinitiators and exposing them to a digital light system (*15*).

Solution-based noncontact processes (*16*), such as inkjet printing, have been used to print molten lead-free solder materials (*17*) and piezoelectric and metal nanoparticles (*18*, *19*). Microwires or micropillars having features of the order of 100 μm were realized in these works (*18*, *19*). Several process parameters (substrate, solvent, and droplet velocity) have also been investigated to address the fabrication constraints and requirements in the printing processes (*20*). Another solution-based nanoparticle printing method, namely, the Aerosol Jet technique, uses a focused sheath of gas to transfer the aerosolized microdroplets containing the nanoparticles. Such a transfer of material allows nanoparticle solutions with a viscosity of up to 1000 centipoise (cP) to be printed using this method. A wide range of feedstock materials can thus be printed; for example, inks and dispersions containing nanoparticles of polymers (*21*), metals (*13*), metal oxides (*22*), and other ceramics (*23*) have been used to print using the Aerosol Jet method.

Here, we use the Aerosol Jet printing technique to deposit aerosolized microdroplets containing metal nanoparticles to assemble the nanoparticles in the form of highly intricate microscale 3D networks, such as microscaffolds/microlattices with nearly fully dense truss elements without the use of any supporting materials. The structural features are shown spanning over five orders of magnitudes in length scale. Furthermore, we were able to controllably engineer the internal porosity and surface topography of the truss elements of the scaffolds through varying sintering conditions (for example, sintering profile and/or power source), thus introducing a hierarchy in porosities within the structure, in addition to that from free-form printing.

RESULTS AND DISCUSSION

Pointwise spatial printing inspired by nature

First, we describe the free-form printing used to obtain the complex hierarchical structures described in this study. The printing process was inspired by similar methods occurring in nature that resulted in

School of Mechanical and Materials Engineering, Washington State University, Pullman, WA 99163, USA.
*Corresponding author. Email: rahul.panat@wsu.edu

complex or elegant 3D architectures. For example, petal-shaped gypsum crystals typically found in the West African deserts and called "Desert Roses" are formed by precipitation and condensation of aerosolized liquid droplets (in a fog) that carry dissolved sulfur compounds. The crystal is then formed in 3D by evaporation of the solvents by the desert heat (*24*, *25*). This process is depicted schematically in Fig. 1A. We adopted this strategy to fabricate 3D microarchitectures in a controlled manner that mimicked the natural process shown in Fig. 1A. We use silver nanoparticles dispersed in an aqueous ethylene glycol solution as a source of building material (see Materials and Methods). An aerosolized fog containing droplets from this solution is then generated from the Aerosol Jet technique and carried toward the heated substrate to build a 3D microarchitecture/microscaffold of silver nanoparticles with truss elements in the air that do not require any supporting material or templating (Fig. 1B). The principle of operation of the Aerosol Jet technique is given in section S1. We use a marked increase in the evaporation rate of the solvent droplets when their diameter is below 50 μm at moderate temperatures to solidify the deposited material (nanoparticle with binders) before the arrival of the successive droplet. A high particle loading ratio (up to about 70% by volume at the time the droplets exit the print head) is used, and the nanoparticles are sintered in the presence of an energy source, such as heat or photonic power. It is noted that this approach is independent of the microdroplet generation method, although we used the Aerosol Jet printing for finer droplet sizes and, hence, features. The achieved microarchitectures and microlattices consist of a network of interconnecting spatial truss elements at various angles to the horizontal that are as thin as 20 μm in diameter and have open void sizes ranging from 100 μm to 1 mm from the printed architectures. To achieve these fine features, precise process control is highly critical. In the next section, we present physical models to predict the required process parameters for the 3D architectures.

Physical model and control parameters

Building a 3D structure in the air with nearly fully dense truss elements without the sacrificial materials relies on accurate fabrication parameter settings, such as platen temperature and droplet loading ratio. Determination of the critical angle of growth and the stability of growing elements are the two main parameters that constrain the geometry of the 3D microscaffolds. To gain an understanding of the two parameters, we first studied the kinematics of the droplet precipitation process to predict the lowest angle of growth in space for the nanoparticle assembly for different droplet heights (measured after drying) as function of the droplet diameter (Fig. 2). The formulation of the model and the resulting equations are derived in section S2. A condensed ink droplet deposited over a ledge and the free-body diagram being considered for the analysis are shown in Fig. 2A. For spherical droplets with a radius of about 20 ± 5 μm and a dried droplet height of 10 to 20 μm, the predicted critical angle of growth is about 35° ± 7° (Fig. 2B). The second significant parameter is the solvent rate of evaporation, which dictates how fast the precipitated droplet dries out. It is desirable to have fast solvent evaporation for the nanoparticle microdroplets above the previously solidified droplet. The evaporation rate and microdroplet half-life time (that is, when the droplet loses half of its volume to evaporation) have been estimated as a function of time

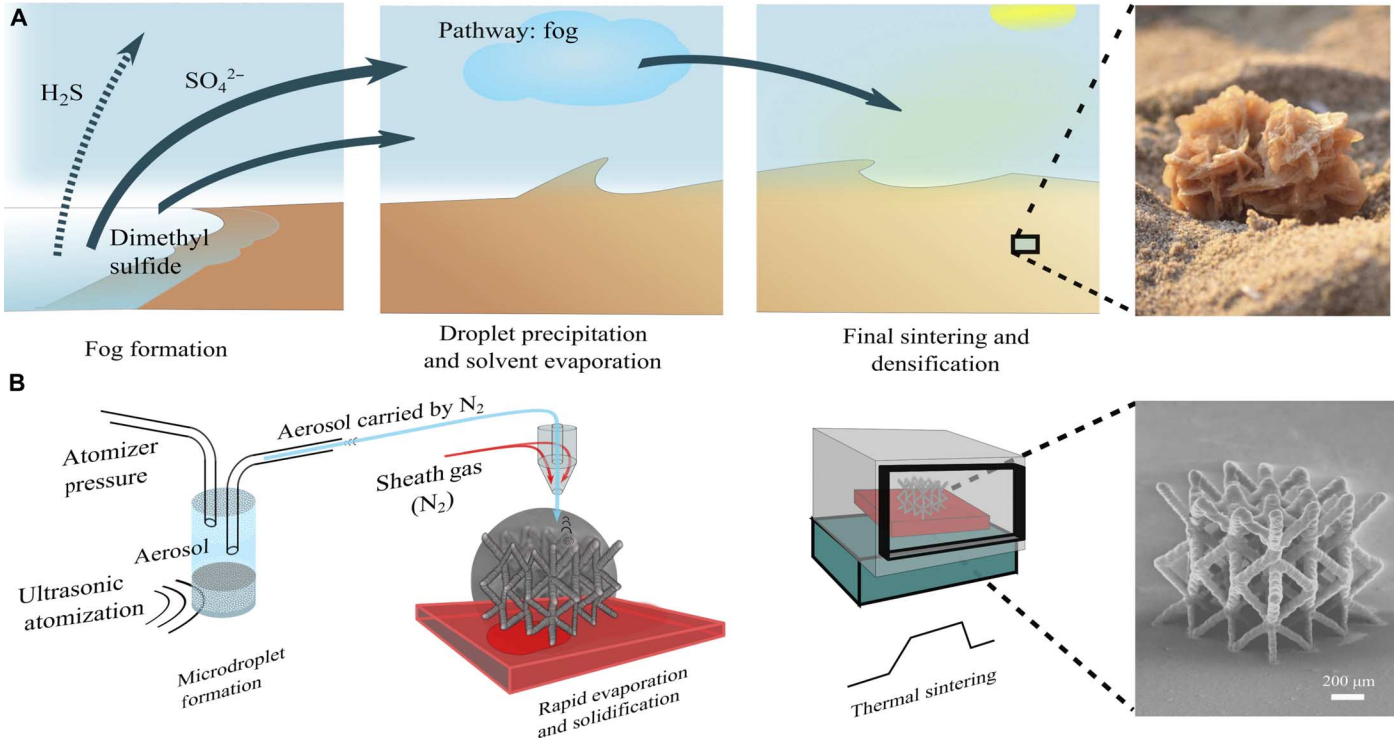

Fig. 1. Analogy of the natural growth of Desert Rose and the 3D buildup of nanoparticles by pointwise printing to realize microarchitectures. (**A**) An illustration of the Desert Rose formation process by condensation of sulfur-containing fog along with the elevated temperature of the desert climate. Desert Rose photo courtesy of O. Apostolidou (reprinted with permission). (**B**) In a process inspired by that shown in (A), we used successive condensation of droplets of nanoparticle ink in the spatial dimension followed by solvent evaporation and sintering to create controlled 3D microarchitectures with hierarchical porosity. The scanning electron microscopy (SEM) image resembles a petal-shaped structure (right). The truss element diameter is about 40 μm.

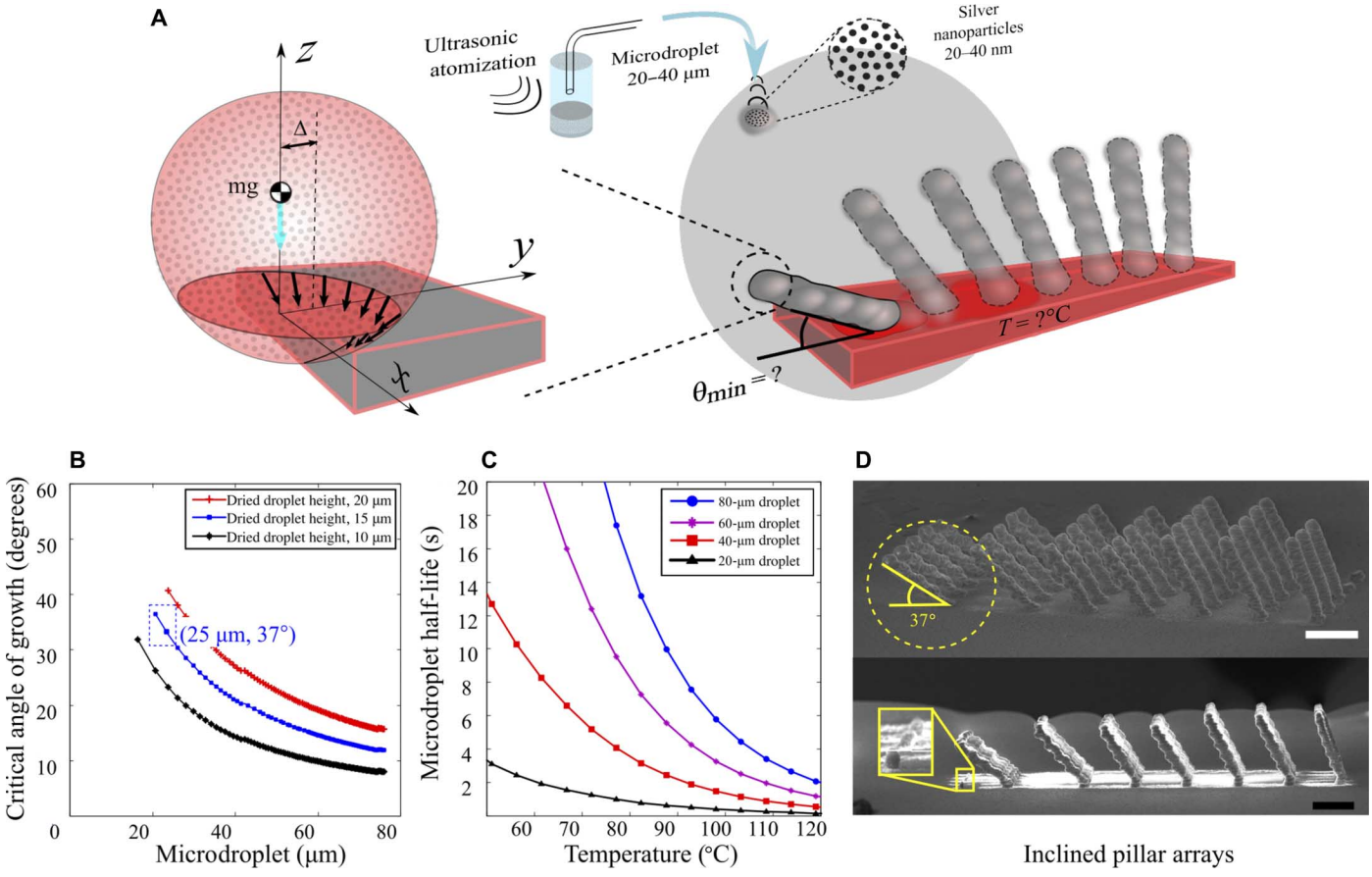

Fig. 2. An illustration of physical models developed to study the stability and control of pointwise printing and their experimental verification. (**A**) A simplified free-body diagram of a critical droplet at the edge of a structure and the illustration of a designed experiment to verify the models. (**B**) The predicted angle of growth as a function of droplet radius for different measured dried droplet heights. (**C**) The half-life time of the microdroplet was numerically calculated by evaporation rate estimation as a function of substrate temperature. (**D**) SEM images showing a series of inclined pillars fabricated at different angles to verify the model predictions. A magnified side view of the last inclined pillar establishes the critical angle (smallest angle to the horizontal for the assembled pillar by this method) at 37° that matches reasonably well with the model prediction. Scale bar, 250 μm.

and temperature (see section S3 for the details of the derivation and Fig. 2C). It is revealed that for temperature ≤100°C, the drying time increases markedly with an increase in the droplet diameter. The above-mentioned results and analyses were verified experimentally by assembling nanoparticles as pillars and successively lowering the angle of growth to find the critical angle at which the droplet would eventually fall down instead of forming the pillar, as shown in Fig. 2D. The critical angle in these experiments was about 37°, in agreement with that predicted in Fig. 2B. Further, the pillars could be realized only at temperatures higher than about 90°C, again in reasonable agreement with the prediction of the evaporation model. The models developed could thus be used to determine the required platen temperature and the stable microdroplet diameters to build a free-standing microarchitecture to fit the specific microdroplet generation method. Next, we use the method to create the unique 3D microarchitectures in two simple manufacturing steps, namely, the deposition of the nanoparticle ink droplets and final sintering.

Three-dimensional hierarchical architectures

Figure 3 (A to C) shows microscale networked lattice structures printed using the above schema having octahedral (Fig. 3, A and C) and hexagonal (Fig. 3B) unit cells, with fullness fractions of 27, 9.5, and 14.5% and structural periodicities of 100, 300, and 200 μm, respectively. The overall length scale of the structures is of the order of a few millimeters. The as-printed microscale scaffolds (before sintering) consisted of nanoparticles dispersed in binders. However, after sintering, the binders are expected to escape, leaving the sintered nanoparticles to form the 3D network in space. Figure 3D shows the scaffold after sintering with the sintered nanoparticles, showing the near-full density of the truss elements. The micrographs in Fig. 3 thus demonstrate scaffold structures with high complexity at length scales described above with nearly fully dense truss elements. Next, we show that nanoparticle sintering conditions can be varied to obtain very low porosities (near-full density) to higher porosities in the truss elements if desired, which gives rise to the hierarchical structures that span over several orders of magnitudes in length scale. We note that hierarchical porosities are observed in naturally developed materials and biological systems that help them tolerate strain (*26*, *27*). The method described in this study offers an excellent opportunity to artificially fabricate such strain-tolerant structures by tailoring porosities from nanoscales (from nanoparticle sintering) to hundreds of micrometers in scale (from the Aerosol Jet printing). For example, Fig. 3 clearly shows the

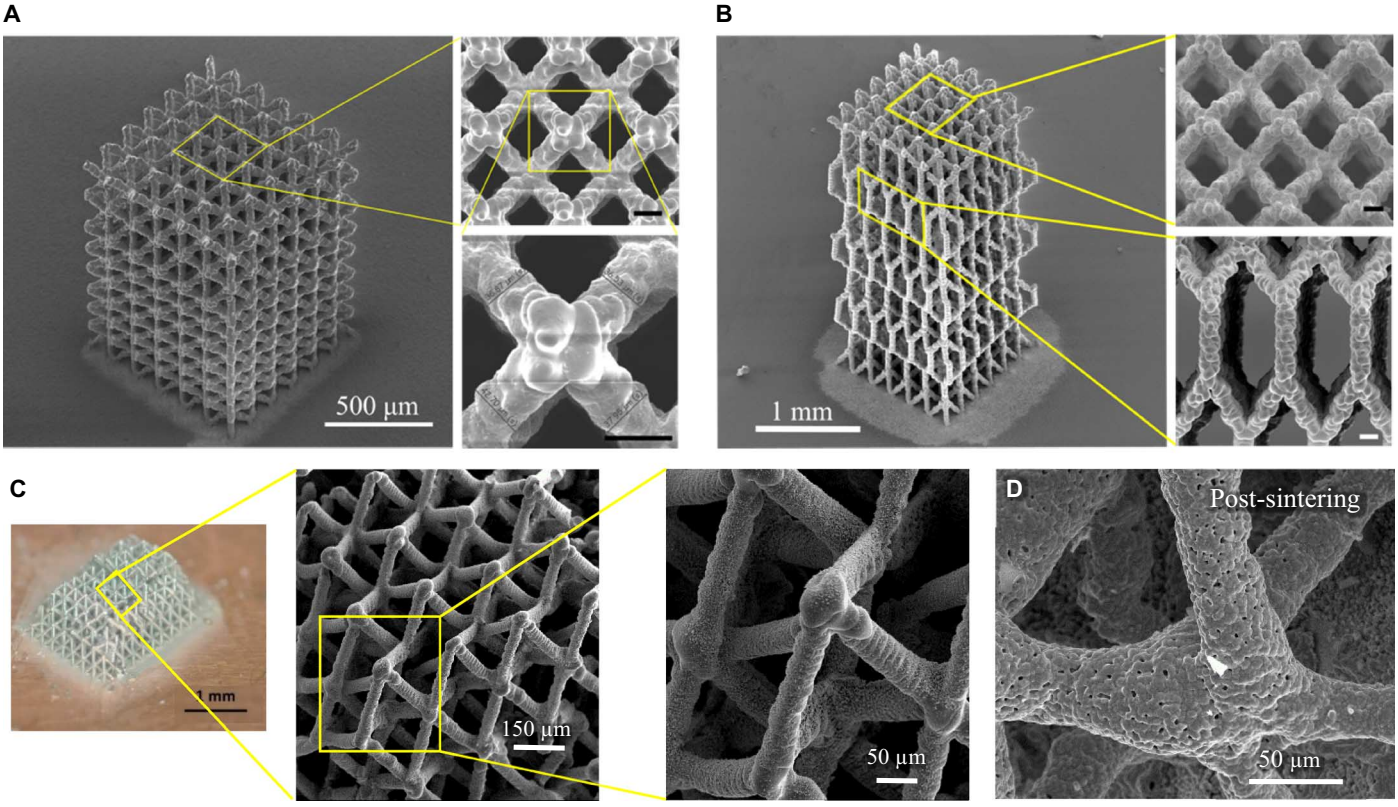

Fig. 3. Pointwise-printed 3D microarchitectures with different network topologies. (**A**) An open octahedral microarchitecture with truss elements having a diameter of about 35 µm. Scale bars, 50 µm. (**B**) Pointwise-fabricated microarchitecture with a combination of octahedral and hexagonal structures. Scale bars, 50 µm. (**C**) Top surface of an octahedral scaffold structure at different magnifications and (**D**) truss elements of the 3D-printed scaffold after binder escape and nanoparticle sintering and possible grain growth.

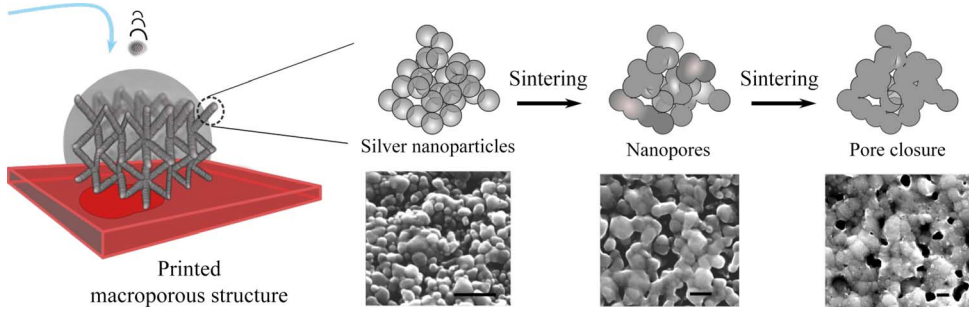

Fig. 4. The pointwise printing in combination with controlled sintering technique. The printed material is designed to contain the first level of macroporosities. Coalescence of sintered nanoparticles starts to form the second level of porosity and could be stopped before pore closure and grain growth. Scale bars, 100 nm.

scaffold with a porosity of the order of 100 to 300 µm through printing in 3D. Because the truss elements are made from nanoparticles and binders when the printing occurs, different sintering conditions can remove the binders and stop the crystal growth before complete pore closure to give them variable densities. The porosities could also be manipulated by using different nanoparticle sizes.

Figure 4 shows a schematic and the micrographs of nanoparticle porosities for silver nanoparticles having diameters in the range of 30 to 50 nm. The pore sizes and length scales of the order of 100 nm are evident. We also used silver flakes of about 1 µm in size and sintered both types of nanoparticles under different conditions. The detailed study of the sintering conditions can be found in section S4, where different levels of porosities are observed for different sintering conditions and two particle sizes, as shown in fig. S4.

To further demonstrate the hierarchical length scales achieved by this technique, we fabricated a variety of micro-architected structures, as shown in Fig. 5. Printed silver lattices with octahedral and hexagonal architectures are shown in Fig. 5A. The truss elements have diameters in the range of 30 to 55 µm, whereas the periodicity of pores from printing is of the order of about 300 µm. The overall scale of the scaffold is over a few millimeters. Figure 5 (B and C) shows features at length scales of hundreds to tens of micrometers, respectively. Figure 5D

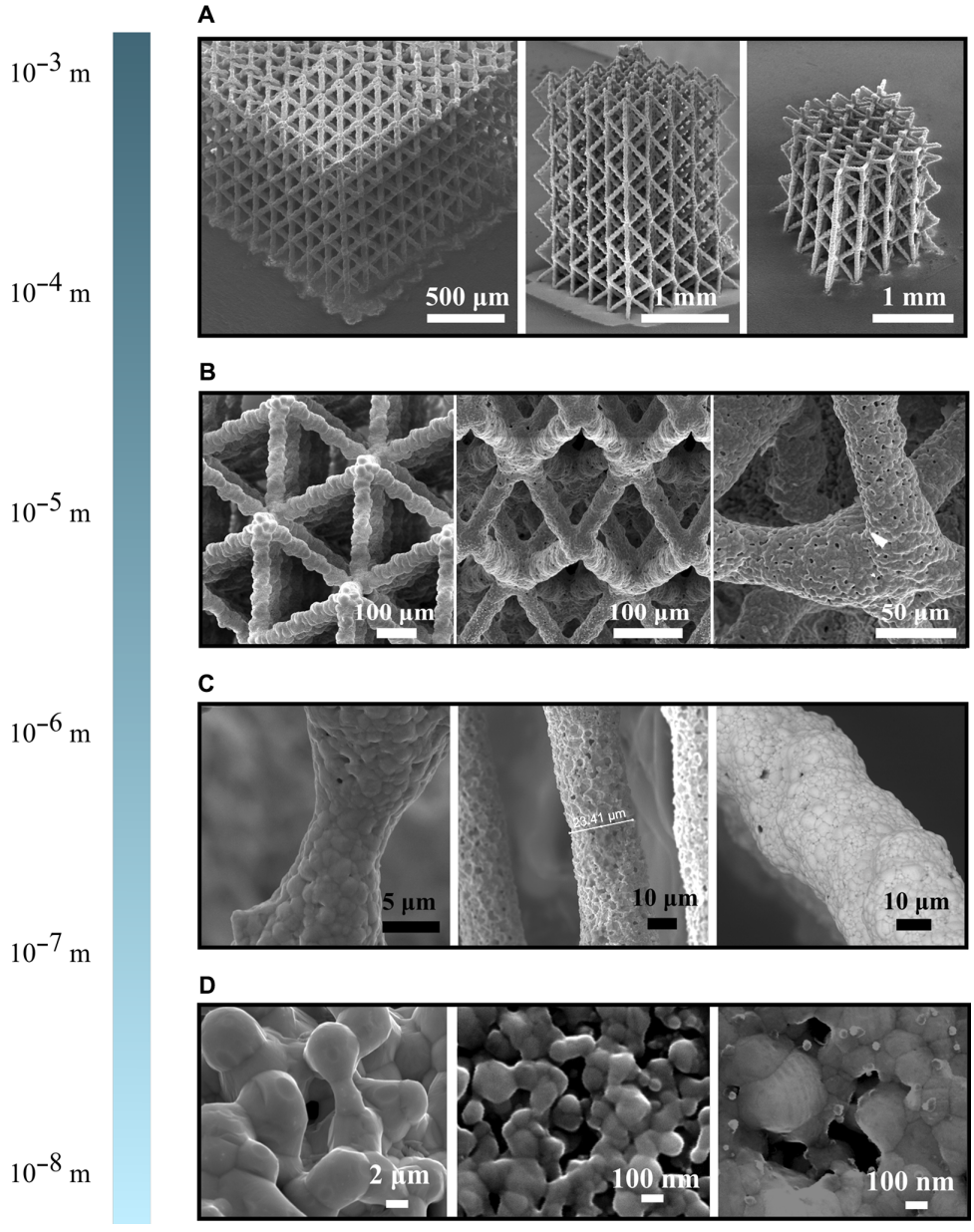

Fig. 5. Pointwise-printed hierarchical materials with 3D microarchitectures having features that span over five orders of magnitudes in length scale. (**A**) SEM images of octahedral and hexagonal microlattices at a bulk view at a length scale of millimeters. (**B**) High aspect ratio truss elements forming the architecture of sintered structures introducing the first level of porosity. (**C**) The engineered surface of truss elements of the lattice induced by different sintering profiles featuring a high level of porosity to near dense materials. (**D**) The final order of controlled surface features and porosity for different sintering temperature profiles that show several microscale to nanoscale voids.

shows a variety of microporous structures that could be achieved by sintering of nanoparticles having a characteristic length scale from several tens of nanometers to a few micrometers. The variety of motifs and the geometry of fabricated structures in Fig. 5 thus demonstrate the precision of pointwise printing in the form of controlled porous microarchitectures that span over five orders of magnitude in size scale.

Applications of the 3D architectures

To demonstrate the applicability of the 3D architectures fabricated in this study, we demonstrated their use as lightweight structural materials. Several microlattices with predetermined void sizes and fullness fractions were fabricated by the method described above using silver nanoparticles with sizes ranging from 30 to 50 nm. The lattices were then compressed in a universal testing machine (see section S5 for details). Figure S5C shows the results for sintered scaffold structures similar to the systems shown in Fig. 3 (A and B), with different fullness fractions and structural periodicities (dimension details are given in fig. S5, A and B, and table S2). We found that these architected materials show a high strength-to-density ratio over a wide range of densities (fig. S5) and occupy a hitherto unrealized area on the Ashby chart and could be comparable with other microlattice metamaterials (fig. S5D) (*8*).

The scaffold structures with hierarchical features described above represent only one of the structures that could be achieved using the proposed fabrication method. In this section, we describe other pointwise printed microstructures and devices to fully describe the use of this method. Figure 6A shows a microscaffold structure having a porous surface with 2- to 5-μm-sized voids. Such morphology is known to be highly amenable for cell proliferation and tissue bonding (*28*). Printed electronics and optoelectronics are current areas of interest, where stretchable spatial interconnects can be of significant use when used in flexible electronics. Figure 6B shows pointwise printed spatial microelectrodes in the form of an accordion shape made from silver nanoparticles between two commercial micro–light-emitting diodes (LEDs). The spatial geometry of these microelectrodes can provide stretchability by deformation in the third dimension. The spatial interconnects are used to control the power supply to the LED, as demonstrated in Fig. 6B. Silver microarchitectures in the form of hollow pillars with outer diameters ranging from 35 to 100 μm are shown in Fig. 6C. Such architectures can be used as heat dissipators in microelectronic devices. Figure 6D shows a high aspect ratio of spiral and thin and thick 3D interconnected truss elements from left to right. A detailed investigation of these areas can potentially lead to separate fields of study and will be part of future investigations.

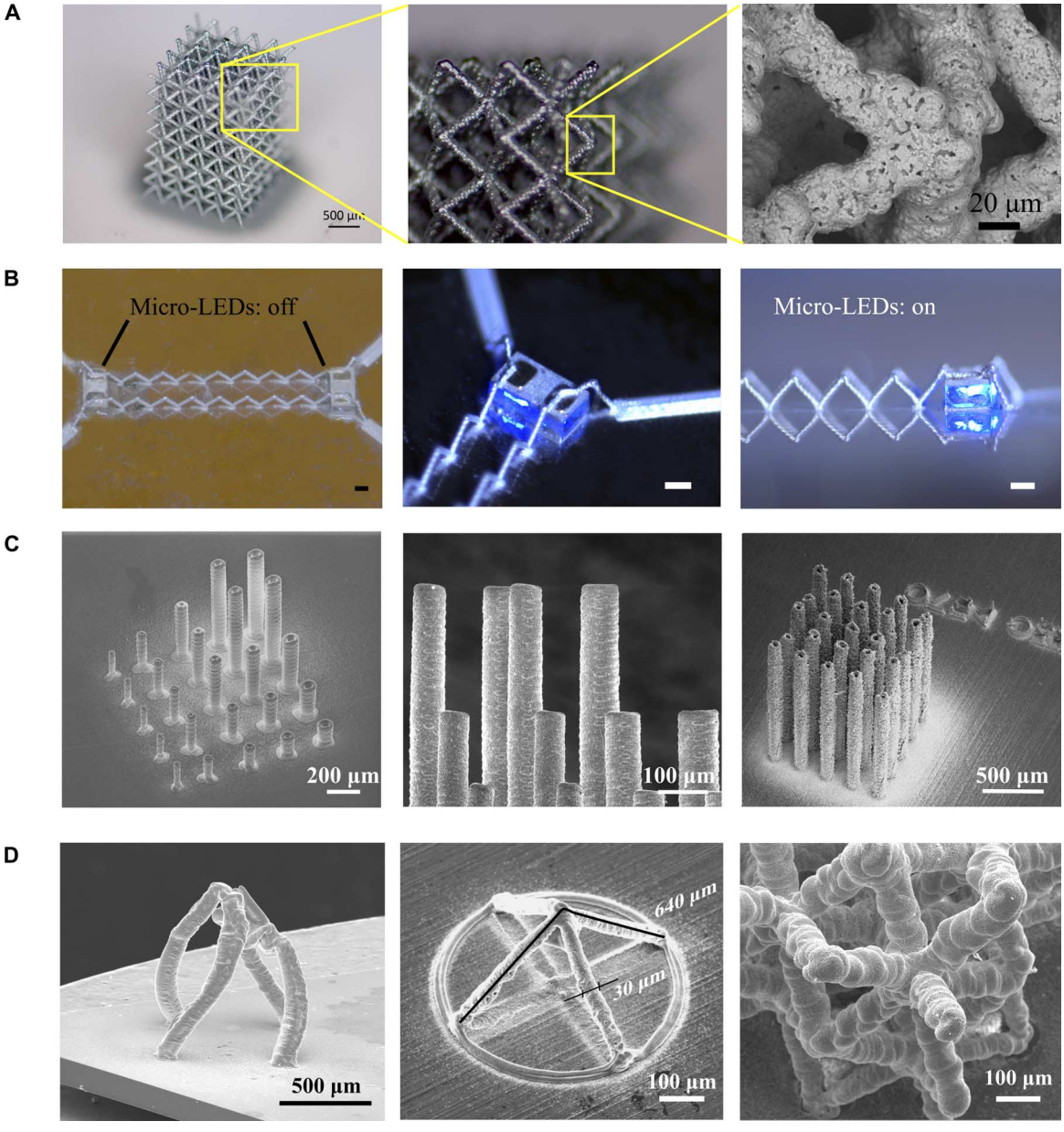

Fig. 6. Demonstration of flexibility of nanoparticle buildup using pointwise printing for a wide range of applications. (**A**) Hierarchical porous scaffold and the topography of porous surfaces that is useful for tissue engineering and cell proliferation. (**B**) Stretchable spatial interconnect assembled between two micro-LEDs. Scale bars, 100 μm. (**C**) SEM image of array of pillars with different diameters (35 to 100 μm) and heights (85 to 500 μm). (**D**) (Left to right) Four spiral high aspect ratio hollow columns forming a dome show the flexibility of this method in fabrication of spatial interconnects. Fine silver interconnects with a thickness of 30 μm and an aspect ratio of over 20.

We note that the physical principles of the method described in this work can be extended to any materials that can be dispersed into a solvent-based slurry in the nanoparticle form. Further, it is possible to create composite micro-architected metamaterials by using nanoparticles of different materials in the ink or by simply changing the ink material anytime during the 3D structure formation. Further, by using heterogeneous particle sizes or different sintering temperatures that selectively allow grain growth, a random variation or a gradient in microstructure can be induced within the truss elements. Another area of future study is the determination of process parameters that affect the printing quality seen in Figs. 2, 3, 5, and 6 in terms of the agglomeration and crystallinity of the printed materials. It is interesting to note that several micropillar compression and microtorsion experiments (*29*, *30*) show that at length scales <100 nm and ~10 μm, the material strength increases compared to that predicted from the conventional Hall-Petch relationship. Such length scales can be found in the truss elements in Figs. 3 and 5 and in the sintered nanoparticles in Fig. 5. The nanoparticle sintering and the 3D microarchitectures can thus be of high interest in this area and will also be part of a future investigation.

CONCLUSIONS

In summary, we have demonstrated a 3D microscale assembly method for nanoparticles to form self-supported complex architectures, such as scaffolds with nearly fully dense truss elements and having length scales over five orders of magnitudes. This is achieved by pointwise spatial printing of the nanoparticle solutions without the use of any templating or supporting materials. Further, by varying the postprocessing conditions, such as sintering, the porosity in the truss elements was varied. We also demonstrate the use of the hierarchical scaffolds as structural materials and that they occupy a hitherto unexplored area on the Ashby chart for the strength of the porous/cellular materials. The hierarchical 3D structures realized by this method have applications in tissue engineering, energy storage, strain-tolerant ultralight materials, microfluidic devices, and microelectronic and optoelectronic devices. This work, in addition to being an important advance in microscale bottom-up assembly of nanoparticles, bridges a length scale gap between nanoscale and microscale architectures and the macroscale device sizes required for real-world applications.

MATERIALS AND METHODS

Materials

Silver nanoparticle ink (PRELECT TPS 30, Clariant) with a density of 1.75 g/cm^3, a viscosity of about 1.5 cP, a particle size of 30 to 50 nm, and a particle loading of 40 ± 2 weight % was used to form the microdroplets for the fabrication of 3D microarchitectures and mesoarchitectures. The solvents used for this ink were deionized water and ethylene glycol. Ethylene glycol acts as a humectant to help in the formation of the 3D architectures. The samples with 3D microarchitecture were fabricated on 10 × 10–mm polished alumina substrates with 96% purity (ALN-101005S1, MTI Corp.). To compare and characterize the porosity as a function of sintering conditions and particle size, we also used silver ink containing 1-μm-sized flakes (Metalon HPS-DEV 79-26-98, NovaCentrix) with 58% particle loading and a viscosity of 150 cP in the form of thin films. Note that the ink containing 1-μm-sized flakes was used only for the porosity study and not to build the 3D architectures.

Microdroplet formation and printing

The Aerosol Jet printer (AJ300, Optomec Inc.) was used to aerosolize the nanoparticle ink. Before printing the structures, the ink material was placed in a tube, which was rotated continuously around its axis for a minimum of 12 hours using a tube roller (MX-T6-S, SCILOGEX) at about 70 rpm to prevent nanoparticle agglomeration within the ink. The silver nanoparticle ink with particle size of 30 to 50 nm was mixed with deionized water at a volume ratio of 3:1 before the atomization process inside the AJ300 machine. An ultrasonic atomizer was used to create the aerosol/mist. The nozzle exit diameter during printing was 100, 150, or 200 μm, depending on the desired truss element diameter. Note that the beam of the aerosol particles was focused to about 10 times smaller in diameter because of the sheath gas when compared to the nozzle diameter according to the manufacturer's observation. The time required to print the scaffold structure varied depending on the platen temperature, the nozzle size, and the structure complexity. For example, the time required to build the scaffold structures similar to that shown in Fig. 3A for a print head was of the order of 40 min. For the printing process, the atomizing flow rate and the sheath gas flow rates were maintained at 28 and 40 sccm (standard cubic centimeter per minute), respectively, which could be slightly altered to achieve the desired printing quality. The platen temperature was set in the range of 90° to 110°C. During printing, the standoff distance between the substrate and the nozzle was kept at about 3 mm and elevated manually every 500 μm of structure growth to avoid physical contact between the nozzle and built structure and to keep the structure in the camera's field of view. The droplet diameter after precipitation was measured using an optical camera (FL3-GE-13S2C, Point Grey). The fullness fractions (volume %) of the samples were estimated using the truss diameters from the SEM images and the total scaffold-lattice structure and were expected to be within ±1%. The fullness fraction does not consider the second-order hierarchical void percentage within the truss elements and is, hence, conservative. The principle of operation of the Aerosol Jet technique is given in section S1.

Measurement of droplet properties

The contact angle measurement was done using a goniometer (VCA Optima and PDAST software, AST Products Inc.). The nanoparticle ink was first dispensed on an alumina substrate to form a 3-mm × 3-mm pad using the Aerosol Jet machine and dried at 80°C for 24 hours. The density of the nanoparticle ink coming out of the nozzle was determined by measuring its volume at a 1-μl accuracy (Hamilton, 81020 1710TTL) and by weighing it in a microbalance (AT201, Mettler-Toledo) at a 0.01-mg accuracy. The density of the droplets exiting the Aerosol Jet nozzle after atomization was determined to be about 6500 ± 500 kg/m^3 for five readings. Further, a sample of concentrated ink with the same density was prepared from the original ink by providing slow solvent evaporation at 60°C and continuous stirring. The concentrated ink droplet was then dispensed onto the previously printed and dried pad, and the contact angle was immediately measured on 10 samples after dispense. The measured contact angle (θ) was 85°. We recognize that the waiting time between dispense and measurement can affect the contact angle as the evaporation proceeds, and this was not considered in the present analysis. The γ_{SL} was measured using the pendant method, along with real-time video analysis with 60 frames/s (VCA Optima and PDAST software, AST Products Inc.). The γ_{SL} was determined to be 7.8 ± 4.4 J/m^2 for 12 readings.

Sintering conditions

To fabricate the 3D microlattices and mesolattices in Figs. 1 to 3, we sintered the samples at 200°C for 30 min in a programmable oven (Neytech Vulcan furnace, model 3-550, Degussa-Ney Dental Inc.). The heating rate was set at 40°C/min. For Fig. 5D (left), the photonic sintering was done using a Xenon Sinteron 2000 (Xenon Corp.) at an energy setting of about 3 J/cm^2 on the equipment. The heating rate and sintering conditions for the experiments used to study the void formation are given in section S4.

SUPPLEMENTARY MATERIALS

Supplementary material for this article is available at http://advances.sciencemag.org/cgi/content/full/3/3/e1601986/DC1

section S1. Aerosol Jet printing technique
section S2. Physical model for the critical angle of growth
section S3. Droplet evaporation rate
section S4. Voids/porosity as a function of the sintering conditions
section S5. Compression tests
fig. S1. An illustration of the Aerosol Jet printing technique.
fig. S2. Schematic of pointwise printing process.
fig. S3. A droplet at the edge of supporting plane.
fig. S4. Porosity evolution for two different particle sizes and sintering conditions.
fig. S5. Mechanical behavior of the 3D-printed hierarchical scaffolds fabricated by the pointwise printing method.
table. S1. Properties of ethylene glycol, the solvent used for the nanoparticle ink.
table. S2. Information about compression test samples and test results.
movie S1. Video showing compressive loading of a 3D microlattice fabricated by the pointwise printing method.
References (*31*–*36*)

REFERENCES AND NOTES

1. J. Banhart, Manufacture, characterisation and application of cellular metals and metal foams. *Prog. Mater. Sci.* **46**, 559–632 (2001).
2. J. Parthasarathy, B. Starly, S. Raman, A design for the additive manufacture of functionally graded porous structures with tailored mechanical properties for biomedical applications. *J. Manuf. Process.* **13**, 160–170 (2011).
3. P. M. Fauchet, Charge- and size-based separation of maeromolecules using novel ultrathin silicon membranes. *Conf. Proc. Lasers Electro-Opt. Soc. Annu. Meet.* **445**, 177–177 (2007).
4. D. Jang, L. R. Meza, F. Greer, J. R. Greer, Fabrication and deformation of three-dimensional hollow ceramic nanostructures. *Nat. Mater.* **12**, 893–898 (2013).
5. J. Seo, T. J. Lee, S. Ko, H. Yeo, S. Kim, T. Noh, S. Song, M. M. Sung, H. Lee, Hierarchical and multifunctional three-dimensional network of carbon nanotubes for microfluidic applications. *Adv. Mater.* **24**, 1975–1979 (2012).
6. H. Zhang, X. Yu, P. V. Braun, Three-dimensional bicontinuous ultrafast-charge and-discharge bulk battery electrodes. *Nat. Nanotechnol.* **6**, 277–281 (2011).
7. G. Nyström, A. Marais, E. Karabulut, L. Wågberg, Y. Cui, M. M. Hamedi, Self-assembled three-dimensional and compressible interdigitated thin-film supercapacitors and batteries. *Nat. Commun.* **6**, 7259–7259 (2015).
8. X. Zheng, H. Lee, T. H. Weisgraber, M. Shusteff, J. DeOtte, E. B. Duoss, J. D. Kuntz, M. M. Biener, Q. Ge, J. A. Jackson, S. O. Kucheyev, N. X. Fang, C. M. Spadaccini, Ultralight, ultrastiff mechanical metamaterials. *Science* **344**, 1373–1377 (2014).
9. X. Zheng, W. Smith, J. Jackson, B. Moran, H. Cui, D. Chen, J. Ye, N. Fang, N. Rodriguez, T. Weisgraber, C. M. Spadaccini, Multiscale metallic metamaterials. *Nat. Mater.* **15**, 1100–1106 (2016).
10. X. Yu, Y.-J. Lee, R. Furstenberg, J. O. White, P. V. Braun, Filling fraction dependent properties of inverse opal metallic photonic crystals. *Adv. Mater.* **19**, 1689–1692 (2007).
11. E. B. D. Jacob J. Adams, T. F. Malkowski, M. J. Motala, B. Yeop Ahn, R. G. Nuzzo, J. T. Bernhard, J. A. Lewis, Conformal printing of electrically small antennas on three-dimensional surfaces. *Adv. Mater.* **23**, 1335–1340 (2011).
12. B. Y. Ahn, E. B. Duoss, M. J. Motala, X. Guo, S.-I. Park, Y. Xiong, J. Yoon, R. G. Nuzzo, J. A. Rogers, J. A. Lewis, Omnidirectional printing of flexible, stretchable, and spanning silver microelectrodes. *Science* **323**, 1590–1593 (2009).
13. M. T. Rahman, L. Renaud, M. Renn, D. Heo, R. Panat, Aerosol based direct-write micro-additive fabrication method for sub-mm 3-D metal-dielectric structures. *J. Micromech. Microeng.* **25**, 107002 (2015).
14. J. A. Lewis, Direct ink writing of 3D functional materials. *Adv. Funct. Mater.* **16**, 2193–2204 (2006).
15. E. Fantino, A. Chiappone, I. Roppolo, D. Manfredi, R. Bongiovanni, C. F. Pirri, F. Calignano, 3D printing of conductive complex structures with in situ generation of silver nanoparticles. *Adv. Mater.* **28**, 3712–3717 (2016).
16. C. Ru, J. Luo, S. Xie, Y. Sun, A review of non-contact micro- and nano-printing technologies. *J. Micromech. Microeng.* **24**, 053001 (2014).
17. C.-H. Wang, H.-L. Tsai, Y.-C. Wu, W.-S. Hwang, Investigation of molten metal droplet deposition and solidification for 3D printing techniques. *J. Micromech. Microeng.* **26**, 095012 (2016).
18. C. Kullmann, N. C. Schirmer, M.-T. Lee, S. H. Ko, N. Hotz, C. P. Grigoropoulos, D. Poulikakos, 3D micro-structures by piezoelectric inkjet printing of gold nanofluids. *J. Micromech. Microeng.* **22**, 055022 (2012).
19. S. H. Ko, J. Chung, N. Hotz, K. H. Nam, C. P. Grigoropoulos, Metal nanoparticle direct inkjet printing for low-temperature 3D micro metal structure fabrication. *J. Micromech. Microeng.* **20**, 125010 (2010).
20. K.-Y. Shin, S.-H. Lee, J. H. Oh, Solvent and substrate effects on inkjet-printed dots and lines of silver nanoparticle colloids. *J. Micromech. Microeng.* **21**, 045012 (2011).
21. J. H. Cho, J. Lee, Y. Xia, B. Kim, Y. He, M. J. Renn, T. P. Lodge, C. Daniel Frisbie, Printable ion-gel gate dielectrics for low-voltage polymer thin-film transistors on plastic. *Nat. Mater.* **7**, 900–906 (2008).
22. K. Hong, S. H. Kim, K. H. Lee, C. Daniel Frisbie, Printed, sub-2V ZnO electrolyte gated transistors and inverters on plastic. *Adv. Mater.* **25**, 3413–3418 (2013).
23. A. M. Sukeshini, P. Gardner, F. Meisenkothen, T. Jenkins, R. Miller, M. Rottmayer, T. L. Reitz, Aerosol jet printing and microstructure of SOFC electrolyte and cathode layers. *ECS Trans.* **35**, 2151–2160 (2011).
24. F. Eckardt, N. Drake, A. Goudie, K. White, H. Viles, The role of playas in pedogenic gypsum crust formation in the Central Namib Desert: A theoretical model. *Earth Surf. Process. Landf.* **26**, 1177–1193 (2001).
25. H. Chen, C. P. Grey, Molten salt synthesis and high rate performance of the "desert- rose" form of $LiCoO_2$. *Adv. Mater.* **20**, 2206–2210 (2008).
26. P. Fratzl, Biomimetic materials research: What can we really learn from nature's structural materials? *J. R. Soc. Interface* **4**, 637–642 (2007).
27. U. G. K. Wegst, H. Bai, E. Saiz, A. P. Tomsia, R. O. Ritchie, Bioinspired structural materials. *Nat. Mater.* **14**, 23–36 (2015).
28. B. Derby, Printing and prototyping of tissues and scaffolds. *Science* **338**, 921–926 (2012).
29. S. Akarapu, H. Zbib, D. Bahr, Analysis of heterogeneous deformation and dislocation dynamics in single crystal micropillars under compression. *Int. J. Plast.* **26**, 239–257 (2010).
30. J. R. Greer, W. D. Nix, Nanoscale gold pillars strengthened through dislocation starvation. *Phys. Rev. B* **73**, 245410 (2006).
31. G. McHale, S. Aqil, N. J. Shirtcliffe, M. I. Newton, H. Y. Erbil, Analysis of droplet evaporation on a superhydrophobic surface. *Langmuir* **21**, 11053–11060 (2005).
32. D. Jakubczyk, G. Derkachov, T. Do Duc, K. Kolwas, M. Kolwas, Coefficients of evapoartion and gas phase diffusion of low-volatility organic solvents in nitrogen from study of evaporating droplets. *J. Phys. Chem. A* **114**, 3483–3488 (2010).
33. M. Inoue, Y. Kondo, T. Inui, An ethylene glycol derivative of boehmite. *Inorg. Chem.* **27**, 215–221 (1988).
34. C. A. Schneider, W. S. Rasband, K. W. Eliceiri, NIH Image to ImageJ: 25 years of image analysis. *Nat. Methods* **9**, 671–675 (2012).
35. M. F. Ashby, The properties of foams and lattices. *Philos. Trans. Math. Phys. Eng. Sci.* **364**, 15–30 (2006).
36. S. D. Papka, S. Kyriakides, In-plane compressive response and crushing of honeycomb. *J. Mech. Phys. Solids* **42**, 1499–1532 (1994).

Acknowledgments: We thank S. Nesaei and A. Gozen for helping with the compression testing experiments at the Washington State University, Pullman. We also thank H. Liu for helping with the measurements of droplet surface energy. **Funding:** The authors gratefully acknowledge financial support from the NSF award no. CMMI-1563546 and the Washington University start-up funds for R.P. **Author contributions:** R.P. came up with the concept and directed the research. M.S.S. developed the fabrication technique and models and carried out the sample preparation and experiments, as well as the imaging and data analysis. C.H. carried out the sintering porosity study. All authors contributed to interpreting the data and preparing and editing the manuscript. **Competing interests:** The authors declare that they have no competing interests. **Data and materials availability:** All data needed to evaluate the conclusions in the paper are present in the paper and/or the Supplementary Materials. Additional data related to this paper may be requested from the authors.

Submitted 22 August 2016
Accepted 1 February 2017
Published 3 March 2017
10.1126/sciadv.1601986

Citation: M. S. Saleh, C. Hu, R. Panat, Three-dimensional microarchitected materials and devices using nanoparticle assembly by pointwise spatial printing. *Sci. Adv.* **3**, e1601986 (2017).